Journal Pre-proof

Optimized acidic fluoride medium ZSM-5 synthesis by using SAPO-34 as an alternative Al source

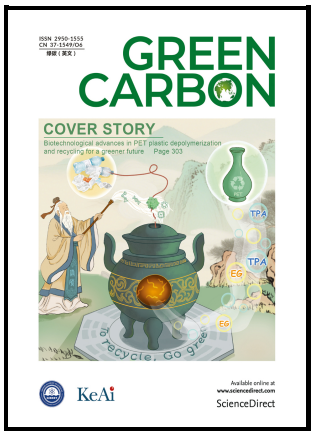

Diandian Shi, Shengjie Ma, Junyan Wu, Ana Palčić, Xiaobing Wang, Valentin Valtchev

PII: S2950-1555(26)00006-6

DOI: https://doi.org/10.1016/j.greenca.2025.11.004

Reference: GREENC149

To appear in: *Green Carbon*

Received date: 3 September 2025
Revised date: 10 November 2025
Accepted date: 30 November 2025

Please cite this article as: Diandian Shi, Shengjie Ma, Junyan Wu, Ana Palčić, Xiaobing Wang and Valentin Valtchev, Optimized acidic fluoride medium ZSM-5 synthesis by using SAPO-34 as an alternative Al source, *Green Carbon,* (2026) doi:https://doi.org/10.1016/j.greenca.2025.11.004

This is a PDF of an article that has undergone enhancements after acceptance, such as the addition of a cover page and metadata, and formatting for readability. This version will undergo additional copyediting, typesetting and review before it is published in its final form. As such, this version is no longer the Accepted Manuscript, but it is not yet the definitive Version of Record; we are providing this early version to give early visibility of the article. Please note that Elsevier's sharing policy for the Published Journal Article applies to this version, see: https://www.elsevier.com/about/policies-and-standards/sharing#4-published-journal-article. Please also note that, during the production process, errors may be discovered which could affect the content, and all legal disclaimers that apply to the journal pertain.

© 2026 Published by Elsevier.

Journal Pre-proof

Optimized acidic fluoride medium ZSM-5 synthesis by using SAPO-34 as an alternative Al source

Diandian Shi[a], Shengjie Ma[a], Junyan Wu[c], Ana Palčić[b], Xiaobing Wang[a,e*], Valentin Valtchev[d,*]

[a] Collaborative Innovation Center of Henan Province for Green Manufacturing of Fine Chemicals, Key Laboratory of Green Chemical Media and Reactions, Ministry of Education, School of Chemistry and Chemical Engineering, Henan Normal University, Xinxiang, Henan 453007, China

[b] Laboratory for Synthesis of New Materials, Division of Materials Chemistry, Ruđer Bošković Institute, Bijenička cesta 54, 10000 Zagreb, Croatia

[c] School of Chemical Engineering, Zhengzhou University, Zhengzhou CN-450001, China

[d] Normandie University, ENSICAEN, UNICAEN, CNRS, Laboratoire Catalyse et Spectrochimie, 6 Marechal Juin, F-14050, Caen, France

[e] Department of Chemical Engineering, Hami Vocational and Technical College, Hami, Xinjiang 839099, China

* Corresponding authors.

E-mail addresses: valentin.valtchev@ensicaen.fr (V. Valtchev), wxb95@163.com (X. Wang)

Journal Pre-proof

ABSTRACT

Incorporating aluminum into the zeolite framework is highly desirable because it generates acid sites, thereby enhancing catalytic performance. However, the introduction of aluminum into a zeolite in a fluoride medium, especially in the strongly acidic regions, is challenging. To address this issue in the synthesis of ZSM-5, SAPO-34, a silicoaluminophosphate zeolite material with strict alternation of -Al-O-P(Si)-O-Al-O- tetrahedra was employed as an alternative aluminum source. Thus, controllable adjustment of the Si/Al ratio of ZSM-5 was achieved by simple variation of the SAPO-

34 amount in the synthesis mixture. Solid-state ^{27}Al and ^{29}Si NMR spectroscopy combined with chemical analyses proves that the resulting MFI-type zeolites contain considerable amounts of framework aluminum. And the Si/Al ratios could be adjusted below 30. Thus, this study provides a simple strategy for one-pot synthesis of heteroatom-containing zeolitic materials for various catalytic and separation applications.

Keywords: Zeolite synthesis, Acidic fluoride medium; Si/Al ratio control; ZSM-5

1 Introduction

Zeolites are heterogeneous catalysts, sorbents, and ion exchangers massively used in process industries. Each year, hundreds of thousands of tons are produced and employed in different applications. The optimization of their synthesis is important not only in terms of efficiency, but also from an environmental point of view since their production is energy-intensive and results in the release of CO_2 and NO_x into the atmosphere [1, 2].

Zeolites are widely used in catalysis, adsorption and separation, and ion exchange because of their uniform pore structures, excellent thermal and hydrothermal stability, and tunable composition and acidity [3-13]. It has been a long time since zeolites were used as the most commonly recognized solid acid catalysts since the early 1960s. In aluminosilicate zeolites, acidic sites are associated with the aluminum present in the zeolite materials [14, 15]. The aluminum atoms incorporated in the zeolite framework introduce negative charges, which are counterbalanced by the extra-framework cations. If such cations are hydrogen ions, then the zeolite is a solid exhibiting Brønsted acidity, while structural defects associated with silanol groups and extra-framework aluminum species usually behave like Lewis acid sites [16-18]. Therefore, we expect that a suitable amount of aluminum can be introduced into zeolites to endow them with appropriate acidic properties. However, for zeolite synthesis in fluoride medium, aluminum ions readily complex with fluorine ions to form AlF_x species, which hinders their incorporation into the zeolite framework and reduces the subsequent formation of

Journal Pre-proof

Brønsted acid sites [19]. Consequently, obtaining Al-rich zeolitic materials in fluoride medium is difficult, which severely limits the synthesis and development of acidic zeolite catalysts [20].

Zeolite syntheses are typically conducted under basic conditions where the OH^- is the mineralizing agent [21-23]. Conventional zeolite syntheses are performed at relatively high pH (> 9) using alkali metals and/or quaternary ammonium cations as structure-directing agents (SDA). While basic (OH^-) medium generally results in faster zeolite crystallization, it simultaneously increases the likelihood of framework defects and crystal intergrowths [24, 25]. A significant breakthrough in the synthesis of zeolites in fluoride medium, pioneered by the researchers at Mulhouse and Valencia, is seen as a milestone in the history of zeolite synthesis [26-28]. Compared to the traditional hydroxide synthesis approach, this innovative approach not only provides a novel mineralizing route but also introduces new possibilities for improving zeolite properties. Higher hydrophobicity, improved thermal/hydrothermal stability, and minimal framework defects have attracted considerable attention from scientists in both academia and industry [29-31]. In addition, fluoride synthesis typically occurs in neutral or weakly acidic conditions, which can, to some extent, prevent the precipitation of metal ions, a phenomenon that often occurs in conventional basic hydroxide media [32, 33]. Therefore, fluoride synthesis is a promising strategy for obtaining specific zeolite catalysts tailored to meet the different demands of various catalytic processes.

Recently, we successfully synthesized MFI-type zeolites in strongly acidic regions, that is, at pH between 2 and 5, which is a leap in the preparation of high-silica zeolites by expanding their synthesis field [34]. However, the materials exhibited especially high silicon-to-aluminum (Si/Al) ratios, that is, the lowest atomic ratio between Si and Al was approximately 150, which is a common phenomenon but also one of the long-standing historical problems for zeolite synthesis in fluoride conditions. To overcome this limitation, we proposed an inter-zeolite transformation strategy in an acidic medium using four diverse low-silicon commercial zeolites as parent sources [35]. This study demonstrates that Al-rich ZSM-5 with a silicon-to-aluminum ratio of 22 can be obtained in a fluoride medium. The presence of extra-framework aluminum was

observed in these samples, which is a drawback in typical acidic catalytic reactions, such as alcohol dehydration. Recently, inspired by the transcription from duplex DNA to RNA, a low-silica Cu-CHA zeolite enriched with Al pairs was reported by using silicoaluminophosphate (SAPO) material (SAPO-18) as seeds [36]. Herein, we selected SAPO-34 as an alternative aluminum carrier for the one-pot incorporation of aluminum into the framework of MFI-type zeolites. SAPO-34 was employed in this study because it exhibits the strict alternation of Al and P in the framework, which makes the aluminum highly reactive after the dissolution of the crystals. Two types of SAPO-34 with different crystal sizes were employed. Using this approach, we achieved controllable silicon-to-aluminum ratios for MFI-type zeolites by adjusting the amount of SAPO-34 used. The Si/Al ratio of the obtained ZSM-5 ranged between 25 and 70, proving the successful in-situ introduction of aluminum into the ZSM-5 framework. This universal strategy can be employed to direct the synthesis of other heteroatom-containing zeolites.

2 Experimental Section

2.1 Chemicals and reagents

All chemicals and reagents were used as purchased without further purification. They were Ludox HS-30 (30 wt% SiO_2, Sigma-Aldrich), Ludox AS-40 (40 wt% SiO_2, Sigma-Aldrich), Tetraethylorthosilicate (TEOS, Sinopharm Chemical Reagent Co., Ltd, 99%), Aluminum isopropoxide (Macklin, AR), Tetraethylammonium hydroxide (TEAOH, 35 wt%, Kente Catalysts Inc.), Phosphoric acid (H_3PO_4, Sinopharm Chemical Reagent Co., Ltd, 85%), Tetrapropylammonium bromide (TPABr, 98%, Macklin), Hydrofluoric acid, (HF, 40%, Sinopharm Chemical Reagent Co., Ltd), Ammonium fluoride (NH_4F, 96%, Sinopharm Chemical Reagent Co., Ltd), Commercial ZSM-5 zeolite (H-type, Si/Al = 23, Nankai University Catalyst Co., Ltd). Deionized water was used in all experiments.

2.2 Synthesis of SAPO-34

2.2.1 Synthesis of nano-sized SAPO-34

Nano-sized SAPO-34 was synthesized according to the recipe: $1Al_2O_3$: $2P_2O_5$: $0.6SiO_2$: $2TEA_2O$: $75H_2O$. Aluminum isopropoxide (8.81 g), tetraethylammonium

hydroxide (35.62 g), deionized water (2.55 g), and TEOS (2.64 g) were mixed at room temperature and stirred overnight. Then, phosphoric acid (9.76 g) was added dropwise (in 1−2 h). The mixture was stirred for another hour. Finally, the obtained precursor was transferred into a 100 mL stainless steel autoclave and subjected to heating at 150 °C for 14 h.

After the hydrothermal treatment, the solid was collected by centrifugation and washed with deionized water until the pH reached neutrality. Then, the washed sample was dried at 80 °C overnight.

2.2.2 Synthesis of micron-sized SAPO-34

Micron-sized SAPO-34 was synthesized as follows: $1Al_2O_3$: $2.5P_2O_5$: $0.6SiO_2$: $2.5TEA_2O$: $92H_2O$. Aluminum isopropoxide (11.54 g), tetraethylammonium hydroxide (58.30 g), and Ludox HS-30 (3.33 g) were mixed at room temperature and stirred for 4 h. Phosphoric acid (15.98 g) was added dropwise (in 1−2 h). The mixture was stirred for another hour. Finally, the obtained precursor was transferred into a 100 mL stainless steel autoclave and subjected to heating at 150 °C for 15 h.

After the hydrothermal treatment, the solid was collected by centrifugation and washed with deionized water until the pH reached neutrality. Then, the washed sample was dried at 80 °C overnight.

Both nano-sized and micron-sized SAPO-34 were calcined in air at 550 °C for 6 h at a rate of 1 °C/min.

2.3 Synthesis of Al-rich ZSM-5

Ludox AS-40 (3 g), calcined nano/micron-sized SAPO-34 (0.3 g), TPABr (1.019 g), and deionized water (16.2 g) were mixed and stirred at room temperature for 3 h. Then, HF (0.4574 g) and NH_4F (0.1618 g) were added to the above solution. After 10 min of stirring, the pH was determined to be 2.72 (nano-sized SAPO-34) and 2.51 (micron-sized SAPO-34) using a METTLER TOLEDO pH meter. Finally, the two mixtures were transferred into a 50 mL stainless steel autoclave and subjected to heating at 160 °C for different periods, ranging between 13 and 30 days. The products were collected via centrifugation and washed with deionized water until the pH reached neutrality. Then, the washed samples were dried at 80 °C overnight. The templates were

Journal Pre-proof

removed by calcining under air at 550 ℃ for 6 h with the rate of 1 °C/min.

The proportion of the calcined SAPO-34 relative to the total weight of the precursor gel was 1.42 wt%, whereas that of SiO_2 was 10 wt%. The molar compositions of these syntheses were as follows: using nano-sized SAPO-34: $1SiO_2$: $0.056Al_2O_3$: $0.048P_2O_5$: 0.18TPABr: 0.44HF: $0.2NH_4F$: $48.4H_2O$ (Si/Al = 8.9) and using micron-sized SAPO-34: $1SiO_2$: $0.062Al_2O_3$: $0.055P_2O_5$: 0.185TPABr: 0.45HF: $0.21NH_4F$: $49.4H_2O$ (Si/Al = 8.1).

2.4 Synthesis of ZSM-5 with different Si/Al ratios

MFI-type zeolites with different Si/Al ratios were successfully synthesized by adjusting the amount of calcined SAPO-34. When the amount of calcined SAPO-34 was 0.15 g, the proportion between the SAPO-34 crystals and the precursor gel was 0.71 wt%. The proportion of calcined SAPO-34 relative to the weight of SiO_2 was 5 wt%. The corresponding gel molar compositions using nano- or micron-sized SAPO-34 were as follows: $1SiO_2$: $0.029Al_2O_3$: $0.024P_2O_5$: 0.18TPABr: 0.45HF: $0.21NH_4F$: $49H_2O$ (Si/Al = 17.2) and $1SiO_2$: $0.031Al_2O_3$: $0.027P_2O_5$: 0.187TPABr: 0.45HF: $0.21NH_4F$: $49.7H_2O$ (Si/Al = 16.1). When the amount of calcined SAPO-34 was 0.075 g, the proportion between SAPO-34 crystals and the precursor gel equalled 0.36 wt%, while the proportion of calcined SAPO-34 relative to the weight of SiO_2 was 2.5 wt%. The corresponding gel molar compositions using nano- or micron-sized SAPO-34 were as follows: $1SiO_2$: $0.014Al_2O_3$: $0.012P_2O_5$: 0.186TPABr: 0.45HF: $0.21NH_4F$: $49.6H_2O$ (Si/Al = 35.7) and $1SiO_2$: $0.016Al_2O_3$: $0.014P_2O_5$: 0.187TPABr: 0.46HF: $0.21NH_4F$: $49.9H_2O$ (Si/Al = 31.3). When the amount of calcined SAPO-34 was 0.0375 g, the proportion of SAPO-34 crystals to precursor gel was 0.18 wt%. The proportion of calcined SAPO-34 relative to the weight of SiO_2 was 1.25 wt%. The corresponding gel molar compositions using nano- or micron-sized SAPO-34 were as follows: $1SiO_2$: $0.007Al_2O_3$: $0.006P_2O_5$: 0.187TPABr: 0.46HF: $0.21NH_4F$: $49.9H_2O$ (Si/Al = 71.4) and $1SiO_2$: $0.008Al_2O_3$: $0.007P_2O_5$: 0.187TPABr: 0.46HF: $0.21NH_4F$: $50H_2O$ (Si/Al = 62.5).

The Si/Al ratios were evaluated using Equation (1) according to the ^{29}Si MAS NMR analysis, and the results are summarized in Table 2.

Journal Pre-proof

$$(Si/Al)_{NMR} = \sum I_{Si(nAl)} / \sum 0.25 n I_{Si(nAl)} \quad (1)$$

where $I_{Si(nAl)}$ is the intensity of the NMR signal attributable to the Si(nAl) units, and n ranges from n = 0 to n = 4.

All of the Si/Al ratios mentioned refer to the atomic ratios.

2.5 Characterization

Powder X-ray diffraction (XRD) data of all samples were collected using a PANalytical B.V. Empyrean powder diffractometer with Cu Kα radiation (λ = 1.5418 Å, 40 kV, 40 mA) over the range of 2θ = 5.0−50.0° with a scanning speed of 0.026°/s. Scanning electron microscopy (SEM) data were acquired using a JEOL JSM7400F microscope and a MIRA-LMH (TESCAN) scanning electron microscope (SEM). Both devices were equipped with field-emission guns. The Si/Al ratios of the samples were determined using a Rigaku ZSX Primus X-ray fluorescence (XRF) spectrometer. The tests were performed using a pressured pellet method. The details are as follows: the sample is pressed into a pellet using boric acid as a backing material at a pressure of 20 tons for 40 s. Quantitative analysis of the Si and Al content in the samples was automatically performed via XRF measurements operated by SQX. Nitrogen adsorption measurements were performed using a Micromeritics ASAP 2040 automated gas adsorption analyzer at 77 K. The calcined samples were outgassed at 250 °C for 12 h before analysis. The microporous volume (V_{mic}, cm^3/g) was obtained from t-plot analysis based on the Harkins-Jura equation. ^{27}Al and ^{29}Si MAS NMR experiments were performed on a Bruker AVANCE III 600 spectrometer equipped with a 4 mm triple resonance probe operating at a resonance frequency of 156.4 and 119.2 MHz, respectively. ^{27}Al MAS NMR spectra were recorded using a small-flip angle technique with a pulse length of 0.5 μs (<π/12), a 1 s recycle delay, and a spinning rate of 14 kHz. ^{29}Si MAS NMR spectra with high-power proton decoupling were recorded at a spinning rate of 10 kHz, a π/4 pulse length of 2.6 μs, and a recycle delay of 60 s. The chemical shifts of ^{27}Al MAS NMR were referenced to 1 mol/L $Al(NO_3)_3$ aqueous solution (0 ppm), and the ^{29}Si MAS NMR chemical shifts were referenced to kaolinite (-91.5 ppm relative to liquid TMS). Thermogravimetric analysis (TGA) was performed

Journal Pre-proof

with a SHI-MADZU DTG-60 thermal analyzer system in 30 mL min^{-1} air flow with a heating rate of 10 ℃/min from 30 to 800 ℃. NH_3-TPD was carried out in a flow system operating at atmospheric pressure. 100 mg sample (60−100 mesh) was loaded into a quartz tube (φ = 4 mm) and dehydrated in He (50 mL/min) at 350 ℃ for 1 h. The sample was then saturated with NH_3 at 100 ℃ and purged with He for 0.5 h. Temperature-programmed desorption was then performed at 10 ℃/min up to 600 ℃. The amount of desorbed NH_3 was monitored using a thermal conductivity detector (TCD).

3 Results and Discussion

Fig. 1a shows the XRD patterns of the as-synthesized nano- and micron-sized SAPO-34 samples. Both of them display the characteristic peaks attributed to the CHA structure. The nano-sized CHA sample exhibits broader XRD peaks and weaker peak intensity than its micron-sized counterpart. This is because of the smaller crystals and lower crystallinity. Fig. 1b represents the XRD patterns of the calcined CHA samples. The CHA structure was maintained after calcination at 550 °C for 6 h at a heating rate of 1 °C/min. Fig. 1c−f shows the SEM micrographs of the as-synthesized nano- and micron-sized samples used in this study. Both of them consist of agglomerated nano-sized crystals.

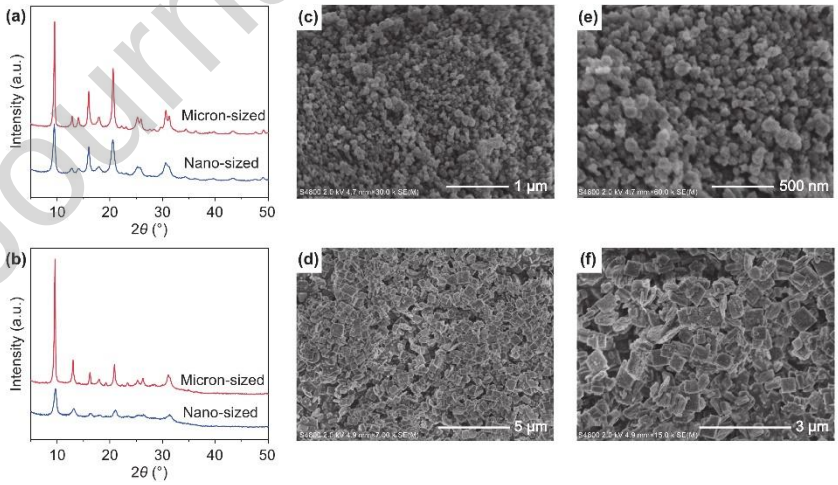

Fig. 1. XRD patterns of as-synthesized (a) & calcined (b) nano-sized and micron-sized SAPO-34. SEM images of as-synthesized nano-sized (c, e) and micron-sized (d, f) SAPO-34.

Journal Pre-proof

Fig. 2a and 2b show the XRD patterns of as-made MFI samples synthesized using the two types of SAPO-34 materials as alternative aluminum sources in strongly acidic fluoride medium after different periods of hydrothermal treatment. After 13 days of crystallization, the characteristic reflections of MFI-type structure appeared, but the crystallinity of both samples was not very high. When the crystallization time was increased to 20 days, the solid products from both systems exhibited higher crystallinity. Furthermore, when we extended the hydrothermal treatment to 30 days, both samples exhibited excellent crystallinity and phase purity. Highly crystalline (20- and 30-day) samples were subjected to SEM analysis. Fig. 2c−f summarizes the SEM results of the MFI samples synthesized with different crystallization periods. The sample synthesized with nano-sized SAPO-34 after 20 days of crystallization showed well-defined elongated crystals of typical MFI morphology with the crystal size of (14−19 × 3−5) μm. In contrast, the sample synthesized with the micron-sized counterpart contained some amorphous material deposited on the surface of the elongated crystals in the form of small particles, which originates from not fully dissolved large crystals. Therefore, it may result in slower nucleation and crystallization. In addition, the ZSM-5 crystals synthesized using micron-sized SAPO-34 showed a modest increase in length and thickness (19−22 × 5−7 μm). When the hydrothermal treatment time reached 30 days, both the samples synthesized using nano-sized and micron-sized SAPO-34 were highly crystalline. Meanwhile, the crystalline products seemed similar in terms of crystal morphology and size (19−22 × 5−7 μm). The crystallization kinetics study was performed to elucidate the synthesis mechanism. As shown in Fig. S1, for both nano- and micron-sized SAPO-34 used as the aluminum source, both systems initially dissolved, as indicated by the amorphous halo after short crystallization. The crystallinity of both systems increased with longer hydrothermal treatment periods. Syntheses using micron-sized SAPO-34 showed slower crystallization kinetics than those using nano-sized ones, which is because larger SAPO-34 crystals dissolve more slowly.

Journal Pre-proof

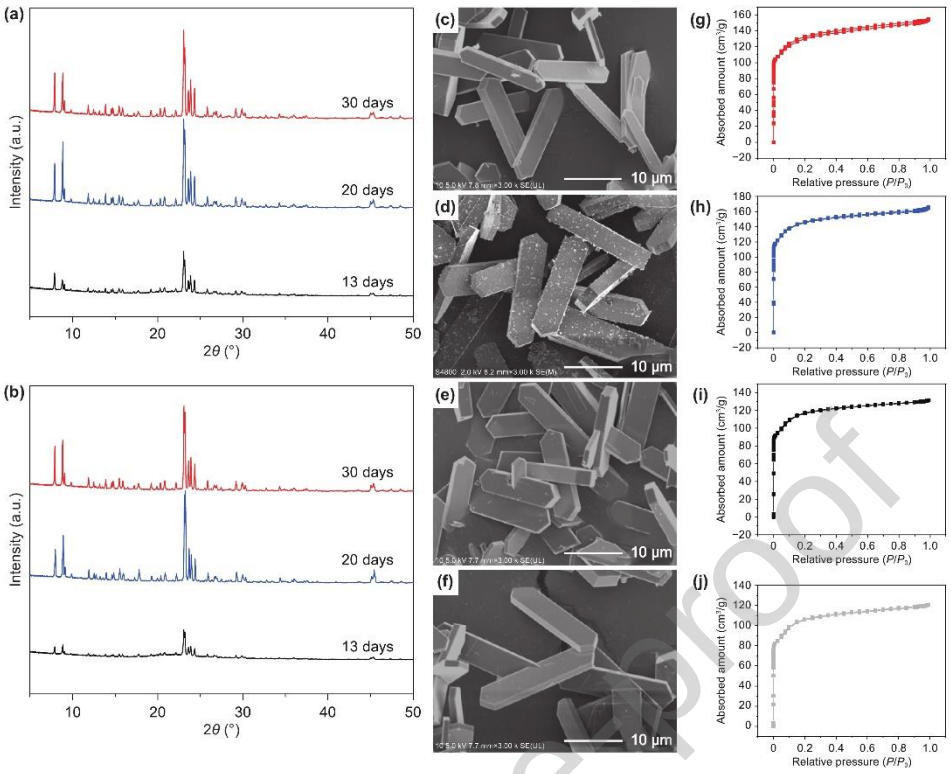

Fig. 2. (a, b) XRD patterns, (c–f) SEM images of as-synthesized ZSM-5 zeolites, and (g–j) N_2 adsorption-desorption isotherms of calcined ZSM-5 zeolites synthesized at 160 ℃ for different periods. (a: using nano-sized SAPO-34; b: using micron-sized SAPO-34). (c, g: using nano-sized for 20 days. e, h: using nano-sized for 30 days. d, i: using micron-sized for 20 days. f, j: using micron-sized for 30 days.)

Fig. 2g–j shows the 77 K N_2 adsorption-desorption results of the four highly crystalline MFI-type samples. All of them exhibited typical type-I isotherms, which showed fast adsorption at low relative pressures and then became steady at high relative pressures. All of the four 20-day and 30-day samples exhibited similar textural parameters, as listed in Table 1, of which the BET specific surface area is above 380 m^2/g and the microporous volume is around 0.16–0.18 cm^3/g. This is consistent with the highly crystalline MFI-type zeolites. Table 1 summarizes the physicochemical characteristics of the highly crystalline series of MFI-type samples, including the XRF results. We can conclude that these samples contained a considerable amount of aluminum, as indicated by Si/Al values lower than 20.

Journal Pre-proof

Table 1. Physicochemical characteristics of the MFI-type samples synthesized with nano- and micron-sized SAPO-34 at 160 °C for different periods.

Sample	Time/day	Si/Al ratio		S_{BET}(m^2/g)	V_{micro}(cm^3/g)
		Initial gel	Product[a]		
Synthesis with nano SAPO-34	20	8.9	18.1	476	0.18
Synthesis with nano SAPO-34	30	8.9	12.6	541	0.18
Synthesis with micron SAPO-34	20	8.1	17.2	426	0.18
Synthesis with micron SAPO-34	30	8.1	19.4	382	0.16

[a] Si/Al ratios of the as-synthesized crystalline products were determined by XRF.

To determine whether the aluminum was successfully incorporated into the framework of the MFI-type zeolites, solid-state ^{27}Al MAS NMR was conducted on the as-made samples, and the results are shown in Fig. 3. Two well-resolved signals could be observed, one of which was split into two peaks at 57.2 and 54.7 ppm, respectively, and another one at -3.6 ppm. The first peak is attributed to framework tetrahedral aluminum, while the peak at -3.6 ppm shows the presence of extra-framework aluminum species. The presence of the extra-framework aluminum stems from the fact that the Si/Al ratios in the initial gel were approximately 9. The minimum Si/Al ratio for the MFI-type zeolite synthesized with TPA^+ is ca. 23-24, which corresponds to 4 TPA^+ cations in a unit cell of 96 T atoms [37].

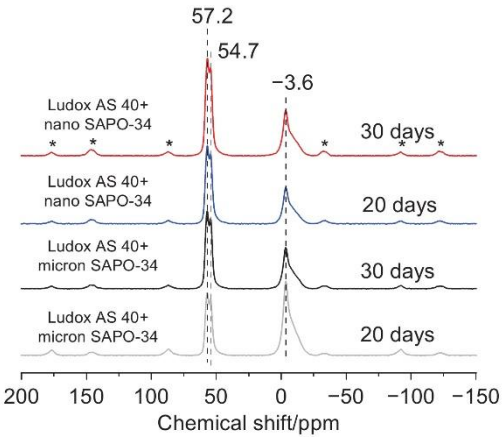

Fig. 3. ^{27}Al MAS NMR spectra of as-synthesized ZSM-5 zeolites after different

crystallization times. Asterisks indicate the spinning sideband.

To remove the possibly unreacted SAPO-34, the as-synthesized samples were treated with 0.1 M HCl solution at room temperature for 3 h, followed by thorough washing using DI water. After calcination, the samples were subjected to ion exchange with 0.5 M NH_4Cl solution at 80 °C for 2 h. The ion-exchanged samples were thoroughly washed and dried at 80 ℃ overnight. The resulting materials were analyzed by solid-state ^{29}Si and ^{27}Al MAS NMR. Fig. 4a shows the ^{27}Al MAS NMR spectra of the treated samples, with well-resolved peaks attributed to framework tetrahedral aluminum only. Fig. 4b exhibits the ^{29}Si MAS NMR results, the peaks at -112 and -114.9 ppm could be attributed to Q^4 (4Si, 0Al) species, and another peak at -105.5 ppm corresponds to Q^3 (3Si, 1Al) or (3Si, 0Al) species [38]. The combined ^{29}Si and ^{27}Al MAS NMR results confirmed the successful incorporation of tetrahedral aluminum into the framework of MFI-type zeolites using SAPO-34 as the aluminum carrier in this strongly acidic synthesis. A commercial ZSM-5 zeolite with Si/Al ratio of 23 was selected for comparison, the XRD and SEM results are shown in Fig. S2. This sample exhibits high crystallinity and micron-sized dimensions. By comparing the ^{29}Si MAS NMR spectra (Fig. S3) of commercial ZSM-5, which possesses a Si/Al ratio similar to that of our synthesized materials, the ratio between the Q^4 and Q^3 species (Q^4/Q^3) provides insights into the condensation degree of the silicon species [39]. The synthesized ZSM-5 afforded a higher Q^4/Q^3 value (6-7) compared to commercial ZSM-5 (2.9), suggesting that the zeolite synthesized under acidic conditions contains fewer defect sites [40].

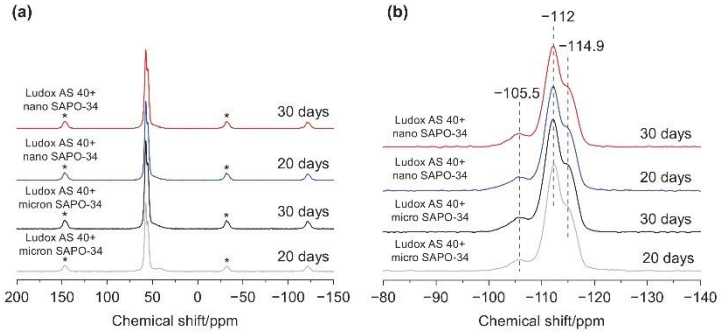

Fig. 4. (a) ^{27}Al MAS NMR and (b) ^{29}Si MAS NMR spectra of MFI zeolites recovered after different crystallization times, treated with HCl and NH_4Cl. The asterisks in the

^{27}Al MAS NMR spectra indicate the spinning sidebands.

To accurately determine the Si/Al ratios of these samples, peak division and integration for the ^{29}Si MAS NMR were performed, and the results are shown in Fig. 5. The Si/Al ratio was evaluated using Equation (1), and the results are summarized in Table 2.

The Si/Al ratios determined based on ^{29}Si MAS NMR were between 20 and 30 and showed high consistency with the XRF results. These results demonstrate that a considerable amount of aluminum was successfully incorporated into the zeolite framework in the strongly acidic fluoride medium using SAPO-34 as an alternative aluminum source.

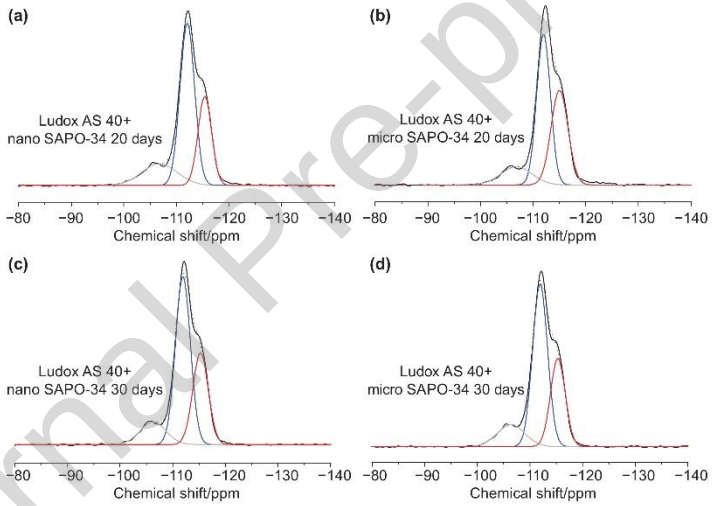

Fig. 5. Deconvoluted ^{29}Si MAS NMR results for treated MFI-type zeolites with different crystallization times.

Table 2. Si/Al ratios of the treated ZSM-5 samples were determined using different characterization methods.

Sample	Time/day	Si/Al ratio		
		Initial gel	Product[a]	Product[b]
Synthesis with nano SAPO-34	20	8.9	22.6	29.3
Synthesis with nano SAPO-34	30	8.9	30.7	26.8
Synthesis with micron SAPO-34	20	8.1	29.9	27.4

Journal Pre-proof

Synthesis with micron SAPO-34	**30**	**8.1**	**28.4**	**26.7**

[a] Calculated according to ^{29}Si MAS NMR tests.

[b] Determined by XRF characterization.

Additionally, 30 days of ZSM-5 synthesized with micron-sized SAPO-34 and commercial ZSM-5 were used for the TG analysis. Fig. S4 shows TG curves of the two ZSM-5 samples after calcination at 550 ℃ in air, and rehydrated at room temperature in air of 65% humidity. Both samples are highly hydrophobic, with water saturation levels of 3.7 and 5.6 wt% at ambient conditions, respectively. Although both samples exhibited similar Si/Al ratios, ZSM-5 synthesized in the acidic medium exhibited significantly higher hydrophobicity. To compare the acid site densities of our ZSM-5 and conventionally synthesized basic samples, we performed the NH_3-TPD on our 30-day samples and their commercial counterparts. The results presented in Fig. S5 demonstrate that our acid-synthesized samples possess acid site densities comparable to those of the commercial samples. All samples contained approximately 40% weak acid sites and 60% strong acid sites. This was consistent with their similar Si/Al ratios.

Furthermore, we successfully synthesized MFI-type zeolites with different Si/Al ratios, ranging from ca. 20−30 to 70, by simply changing the addition amount of calcined nano/micron-sized SAPO-34 during precursor preparation. Fig. S6, S8, S10, and S12 show the XRD patterns of as-synthesized MFI-type zeolites synthesized with various amounts of nano/micron-sized SAPO-34 after 20 and 30 days of hydrothermal treatment, respectively. All samples exhibited characteristic peaks attributed to MFI-type zeolites with high crystallinity and purity. Fig. S7, S9, S11, and S13 show the SEM images of the series of ZSM-5 crystals with a size in the (18−28 × 3−5) μm range. By combining these results, we found that when the Si/Al ratio of the precursor was as high as 16, both types of SAPO-34 could direct the formation of highly crystalline MFI-type products after 20 days of crystallization. Therefore, we chose six calcined samples, aged for 20 days, for the 77 K N_2 adsorption-desorption analysis. Fig. S14 shows the N_2 adsorption-desorption isotherms of six samples with different Si/Al ratios, all of which display typical type-I isotherms characteristic of microporous properties. Table 3

summarizes the textural parameters and the XRF results. All samples exhibit a high surface area, with a BET surface area of around 400 m^2/g and a micropore volume of approximately 0.16 cm^3/g. These results demonstrated the excellent crystallinity of the materials obtained. The X-ray fluorescence spectroscopy results of these as-synthesized samples exhibited higher values than those of the precursor, which could be explained by the faster dissolution rate of the SAPO material in the synthesis precursor. Moreover, we obtained MFI-type zeolites with Si/Al ratios between 25 and 70 in this acidic fluoride medium. Collectively, these results demonstrate flexible control of the Si/Al ratio in ZSM-5 under strongly acidic fluoride-mediated conditions, which is important for tuning acidity to meet specific catalytic requirements.

Table 3. Physicochemical characteristics of the MFI-type samples synthesized with nano & micron-sized SAPO-34 at 160 °C for 20 days.

Sample	Si/Al ratio		$S_{BET}(m^2/g)$	$V_{micro}(cm^3/g)$
	Initial gel	Product[a]		
Synthesis with nano SAPO-34	17.2	36.8	409	0.17
	35.7	43.1	416	0.17
	71.4	62.9	392	0.16
Synthesis with micron SAPO-34	16.1	37.5	416	0.17
	31.3	42.9	391	0.16
	62.5	63.5	411	0.17

[a] Si/Al ratios of the as-synthesized crystalline products were determined by XRF.

4 Conclusion

In summary, we demonstrated that SAPO-34 can serve as an effective aluminum source for the synthesis of Al-rich ZSM-5 zeolites in an acidic fluoride medium. Through combined solid-state ^{29}Si and ^{27}Al MAS NMR and chemical analyses, we found that the Si/Al ratio of the zeolites could be tuned, with the lowest ratio being ca. 25. A series of ZSM-5 samples with controllable Si/Al ratios ranging from 25 to 70 were obtained.

This facile approach offers great potential for introducing diverse heteroatom-containing zeolites with various structures, which may meet the challenges existing in different specific catalytic processes.

Journal Pre-proof

Author contributions

Diandian Shi: Writing the original draft, review and editing, funding acquisition, conceptualization, data curation, formal analysis, investigation, methodology, software, and validation. Shengjie Ma: Investigation and validation. Junyan Wu: Software and validation. Ana Palčić: Writing, review and editing. Xiaobing Wang: Writing, review and editing, formal analysis, resources, and supervision. Valtchev Valentin: Writing, review and editing, resources, supervision, project administration, and funding acquisition.

Declaration of competing interest

The authors declare that they have no known competing financial interests or personal relationships that could have appeared to influence the work reported in this paper.

Acknowledgements

This work is sponsored by the Natural Science Foundation of Henan Province (252300420463), Natural Science Foundation of Shandong Province (ZR2023QB168), and Qingdao Postdoctoral Support (QDBSH20230101015). The ZeoMat Group acknowledges the support from Shandong Energy Institute (SEI S202107), China and the Natural Science Foundation of Shandong Province (ZR2022MB053 and ZR2022QB216), China.

References

[1] Y. Li, L. Li, J.H. Yu, Applications of zeolites in sustainable chemistry, Chem 3 (2017) 928-949.

[2] Q.L. Lang, P. Lu, X.B. Yang, V. Valtchev, Zeolites for the environment, Green Carbon 2 (2024) 12-32.

[3] A. Corma, Inorganic solid acids and their use in acid-catalyzed hydrocarbon reactions, Chem. Rev. 95 (1995) 559-614.

[4] M.E. Davis, Ordered porous materials for emerging applications, Nature 417 (2002) 813-821.

Journal Pre-proof

[5] S. Mintova, M. Jaber, V. Valtchev, Nanosized microporous crystals: emerging applications, Chem. Soc. Rev. 44 (2015) 7207-7233.

[6] J. Li, Z.R. Gao, Q.F. Lin, C.X. Liu, F.X. Gao, C. Lin, S.Y. Zhang, H. Deng, A. Mayoral, W. Fan, S. Luo, X.B. Chen, H. He, M.A. Camblor, F.J. Chen, J.H. Yu, A 3D extra-large-pore zeolite enabled by 1D-to-3D topotactic condensation of a chain silicate, Science 379 (2023) 283-287.

[7] P. Lu, J.Y. Xu, Y.Q. Sun, R. Guillet-Nicolas, T. Willhammar, M. Fahda, E. Dib, B. Wang, Z.X. Qin, H.Y. Xu, J. Cho, Z.P. Liu, H.J. Yu, X.B. Yang, Q.L. Lang, S. Mintova, X.D. Zou, V. Valtchev, A stable zeolite with atomically ordered and interconnected mesopore channel, Nature 636 (2024) 368-373.

[8] A.J. Mallette, K. Shilpa, J.D. Rimer, The current understanding of mechanistic pathways in zeolite crystallization, Chem. Rev. 124 (2024) 3416-3493.

[9] L.J. Liu, J.Y. Lu, Y.H. Yang, W. Ruettinger, X.H. Gao, M. Wang, H. Lou, Z.D. Wang, Y.F. Liu, X. Tao, L.N. Li, Y. Wang, H.J. Li, H. Zhou, C.T. Wang, Q.S. Luo, H.X. Wu, K.D. Zhang, J.B. Ma, X.M. Cao, L. Wang, F.S. Xiao, Dealuminated Beta zeolite reverses ostwald ripening for durable copper nanoparticle catalysts, Science 383 (2024) 94-101.

[10] H. Lee, J. Shin, K. Lee, H.J. Choi, A. Mayoral, N.Y. Kang, S.B. Hong, Synthesis of thermally stable SBT and SBS/SBT intergrowth zeolites, Science 373 (2021) 104-107.

[11] L.B. Deng, Z.Y. Wang, X. Yu, C.Z. Qiao, S.S. Zhou, Q. Deng, Y. Zhao, Y.J. Tian, Brønsted Acid-Triggered Fast Synthesis Pathway of Furfural to Ethyl Levulinate by PtZn Supported on ZSM-5 Nanosheets, ACS Catal. 14 (2024) 16748-16758.

[12] Y.J. Tian, L.H. Guo, C.Z. Qiao, Z.X. Sun, Y. Yamauchi, S.D. Liu, Dynamics-driven tailoring of sub-nanometric Pt-Ni bimetals confined in hierarchical zeolite for catalytic hydrodeoxygenation, Appl. Catal. B: Environ. 336 (2023) 122945.

[13] Y.J. Tian, H.N. Duan, B.F. Zhang, S.Y. Gong, Z.J. Lu, L. Dai, C.Z. Qiao, G.Z. Liu, Y. Zhao, Template Guiding for the Encapsulation of Uniformly Subnanometric Platinum Clusters in Beta-Zeolites Enabling High Catalytic Activity and Stability, Angew. Chem. Int. Ed. 60 (2021) 21713-21717.

Journal Pre-proof

[14] A. Palčić, V. Valtchev, Analysis and control of acid sites in zeolites, Appl. Catal. A: Gen. 606 (2020) 117795.

[15] N. Katada, K. Suzuki, T. Noda, G. Sastre, M. Niwa, Correlation between brønsted acid strength and local structure in zeolites, J. Phys. Chem. C 113 (2009) 19208-19217.

[16] B. Louis, L. Kiwi-Minsker, Synthesis of ZSM-5 zeolite in fluoride media: an innovative approach to tailor both crystal size and acidity, Microporous Mesoporous Mater. 74 (2004) 171-178.

[17] M. Ravi, V.L. Sushkevich, J.A. van Bokhoven, Towards a better understanding of lewis acidic aluminium in zeolites, Nat. Mater. 19 (2020) 1047-1056.

[18] F.J. Yi, Y.L. Chen, Z.C. Tao, C.X. Hu, X.F. Yi, A.M. Zheng, X.D. Wen, Y.F. Yun, Y. Yang, Y.W. Li, Origin of weak lewis acids on silanol nests in dealuminated zeolite Beta, J. Catal. 380 (2019) 204-214.

[19] R.D. Gougeon, E.B. Brouwer, P.R. Bodart, L. Delmotte, C. Marichal, J.M. Chézeau, R.K. Harris, Solid-state NMR studies of the as-synthesized $AlPO_4$-5/TPAF microporous aluminophosphate, J. Phys. Chem. B 105 (2001) 12249-12256.

[20] T. Moteki, R.F. Lobo, A general method for aluminum incorporation into high-silica zeolites prepared in fluoride media, Chem. Mater. 28 (2016) 638-649.

[21] R.M. Barrer, 33. Synthesis of a zeolitic mineral with chabazite-like sorptive properties, J. Chem. Soc. 33 (1948) 127-132.

[22] R.M. Barrer, Zeolites and their synthesis, Zeolites 1 (1981) 130-140.

[23] G.D. Feng, P. Cheng, W.F. Yan, M. Boronat, X. Li, J.H. Su, J.Y. Wang, Y. Li, A. Corma, R.R. Xu, J.H. Yu, Accelerated crystallization of zeolites via hydroxyl free radicals, Science 351 (2016) 1188-1191.

[24] I.C. Medeiros-Costa, E. Dib, N. Nesterenko, J.P. Dath, J.P. Gilson, S. Mintova, Silanol defect engineering and healing in zeolites: opportunities to fine-tune their properties and performances, Chem. Soc. Rev. 50 (2021) 11156-11179.

[25] M.A. Shah, T. Nagornyy, S.E. Aiwekhoe, S. Hong, N.H. Huy Tran, S. Luo, Z. Chen, S.M. Auerbach, W. Fan, Rapid crystallization of zeolites with controllable defects:

Journal Pre-proof

disentangling fluoride concentration and pH using NH_4F, Cryst. Growth Des. 25 (2025) 1821-1832.

[26] J.L. Guth, P. Caullet, Synthèse des zéolites. Perspectives d'avenir, J. Chim. Phys. 83 (1986) 155-175.

[27] J.L. Guth, L. Delmonte, M. Soulard, B. Brunard, J.F. Joly, D. Espinat, Synthesis of Al,Si MFl-type zeolites in the presence of F^- anions: structural and physicochemical characteristics, Zeolites 12 (1992) 929-935.

[28] M.A. Camblor, A. Corma, S. Valencia, Synthesis in fluoride media and characterisation of aluminosilicate zeolite beta, J. Mater. Chem. 8 (1998) 2137-2145.

[29] C.A. Fyfe, D.H. Brouwer, A.R. Lewis, J.M. Chézeau, Location of the fluoride ion in tetrapropylammonium fluoride silicalite-1 determined by $^{1}H/^{19}F/^{29}Si$ triple resonance CP, REDOR, and TEDOR NMR experiments, J. Am. Chem. Soc. 123 (2001) 6882-6891.

[30] Z.X. Qin, L. Lakiss, L. Tosheva, J.P. Gilson, A. Vicente, C. Fernandez, V. Valtchev, Comparative study of nano-ZSM-5 catalysts synthesized in OH^- and F^- media, Adv. Funct. Mater. 24 (2014) 257-264.

[31] X.B. Yang, E. Dib, Q.L. Lang, H.L. Guo, G.Y. Fu, J. Wang, Q.S. Yi, H.N. Zhao, V. Valtchev, Silicalite-1 formation in acidic medium: synthesis conditions and physicochemical properties, Microporous Mesoporous Mater. 329 (2022) 111537.

[32] H. Li, J.Y. Yu, K. Du, W.Y. Li, L. Ding, W. Chen, S.H. Xie, Y.H. Zhang, Y. Tang, Synthesis of ZSM-5 zeolite nanosheets with tunable silanol nest contents across an ultra-wide pH range and their catalytic validation, Angew. Chem. Int. Ed. 63 (2024) e202405092.

[33] Y. Zhou, J.L. Zhang, L. Wang, X.L. Cui, X.L. Liu, S.S. Wong, H. An, N. Yan, J.Y. Xie, C. Yu, P.X. Zhang, Y.H. Du, S.B. Xi, L.R. Zheng, X.Z. Cao, Y.J. Wu, Y.X. Wang, C.Q. Wang, H.M. Wen, L. Chen, H.B. Xing, J. Wang, Self-assembled iron-containing mordenite monolith for carbon dioxide sieving, Science 373 (2021) 315-320.

[34] D.D. Shi, K.G. Haw, C. Kouvatas, L.X. Tang, Y.Y. Zhang, Q.R. Fang, S.L. Qiu, V.

Journal Pre-proof

Valtchev, Expanding the synthesis field of high-silica zeolites, Angew. Chem. Int. Ed. 59 (2020) 19576-19581.

[35] D.D. Shi, G.Y. Fu, A. Omran, K.G. Haw, L.K. Zhu, R.Q. Ding, Q.L. Lang, S.X. Wang, Q.R. Fang, S.L. Qiu, X.B. Yang, V. Valtchev, Acidic properties of Al-rich ZSM-5 crystallized in strongly acidic fluoride medium, Microporous Mesoporous Mater. 358 (2023) 112332.

[36] Y.Z. Wang, J.F. Han, M.Y. Chen, W.T. Lv, P.T. Meng, W. Gao, X.J. Meng, W.B. Fan, J. Xu, W.F. Yan, J.H. Yu, Low-silica Cu-CHA zeolite enriched with Al pairs transcribed from silicoaluminophosphate seed: synthesis and ammonia selective catalytic reduction performance, Angew. Chem. Int. Ed. 62 (2023) e202306174.

[37] S. Al‐Nahari, E. Dib, C. Cammarano, E. Saint‐Germes, D. Massiot, V. Sarou‐Kanian, B. Alonso, Impact of Mineralizing Agents on Aluminum Distribution and Acidity of ZSM‐5 Zeolites, Angew. Chem. Int. Ed. 62 (2023) e202217992.

[38] W.J. Dai, L.N. Zhang, R.Z. Liu, G.J. Wu, N.J. Guan, L.D. Li, Plate-Like ZSM-5 zeolites as robust catalysts for the cracking of hydrocarbons, ACS Appl. Mater. Interfaces 14 (2022) 11415-11424.

[39] Y.X. Hou, X.Y. Li, M.H. Sun, C.F. Li, S.U.H. Bakhtiar, K.H. Lei, S. Yu, Z. Wang, Z.Y. Hu, L.H. Chen, B.L. Su, The effect of hierarchical single-crystal ZSM-5 zeolites with different Si/Al ratios on its pore structure and catalytic performance, Front. Chem. Sci. Eng. 15 (2020) 269-278.

[40] Q.S. Yi, L. Lin, H.W. Geng, S.H. Chen, Y.C. Shao, P. He, Z.F. Liu, H.M. Xu, T.H. Chen, Y.S. Liu, V. Valtchev, Benefits of H-ZSM-5 zeolite from fluoride-mediated acidic synthesis for liquid-phase conversion of cyclohexanol, Chin. J. Catal. 74 (2025) 97-107.

Journal Pre-proof

Graphical abstract

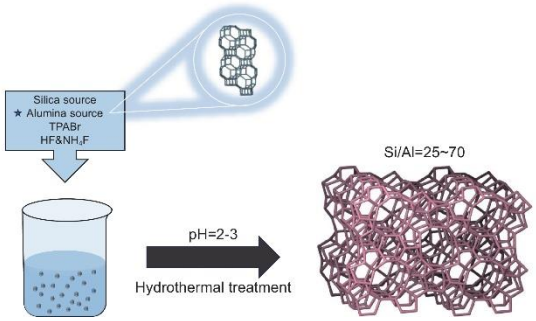

Journal Pre-proof

Journal Pre-proof

Declaration of interests

☐ The authors declare that they have no known competing financial interests or personal relationships that could have appeared to influence the work reported in this paper.

☒ The authors declare the following financial interests/personal relationships which may be considered as potential competing interests:

Has patent pending to. If there are other authors, they declare that they have no known competing financial interests or personal relationships that could have appeared to influence the work reported in this paper.

Journal Pre-proof